PIV and CFD Study on the Axial and Transverse Velocity Distributions in a 19-Pin Wire-wrapped Fuel Bundle Channel*

Dajun Fan,[1,2,3] Rongjie Li,[1,2,3] Chengwen Qiang,[1,2] Minghan He,[1,2]
Lu Liu,[1,2] Dawei Wang,[1,2] Sicheng Wang,[1,2,†] and Han Wang[4,‡]

[1]*Institute of Modern Physics, Chinese Academy of Sciences, Lanzhou 730000, China*
[2]*School of Nuclear Science and Technology, University of Chinese Academy of Sciences, Beijing 100049, China*
[3]*Huizhou Ion Science Research Center, Huizhou 516003, China*
[4]*North China Electric Power University, Beijing 102206, China*

China initial Accelerator Driven System (CiADS) holds immense promise for transmuting nuclear wastes and enhancing the nuclear fuel's utilization rate. A study on the flow characteristics in reactor fuel assemblies is crucial for its design and safety analysis. In this study, a Visual Hydraulic ExperimentaL Platform (VHELP) was built to study the flow velocity distribution in a fuel assembly of CiADS, employing polymethyl methacrylate and a 62.932 wt% sodium iodide solutions as the material of the test section and refractive index matching fluid. Particle image velocimetry (PIV) and FLUENT were used to investigate the axial and transverse velocity distribution within the axial height of 2.25-3.25 pitches (H) and 3.75-4.75 H in 19-pin wire-wrapped fuel bundle channels. The findings reveal that the Shear Stress Transport (SST) k-ω model can accurately describe the velocity distribution in a wire-wrapped fuel assembly, and the transverse and axial periodicity of velocity distribution was one pitch. The flow velocity distribution patterns were unchanged with various Reynolds numbers. The patterns of velocity contour images on gaps 1 through 5 at 2.25-3.25 H were symmetrical to that at 3.75-4.75 H on gaps 5 through 1, respectively. The value of axial velocities and root mean square (RMS) transverse velocities proportionally increased with the increase of Reynolds numbers. Normalized transverse velocity changed in a cosine function, with a maximum value of about 40% and a peak occurring at a position slightly behind 3/4 H. The cross-flow around wire-wrap spacers enhanced and there was a deviation in the velocity direction. These results can help researchers deepen the understanding of flow velocity distribution in wire-wrapped fuel bundles, and advancing research on the cross-flow characteristics of lead-cooled fast reactors.

Keywords: wire-wrap spacer, bundle channel, cross-flow, refractive index matching, particle image velocimetry, subchannel analysis

I. INTRODUCTION

Lead-cooled fast reactor (LFR) has excellent neutronic characteristics, thermal safety characteristics, and anti-nuclear proliferation capabilities, and it has been selected as the reactor type of the China initial Accelerator Driven System (CiADS) [1–3]. The CiADS, designed to transmute long-lived high radioactive nuclear wastes, includes three main components: a linear accelerator, a spallation target, and a subcritical reactor. As a typical positioning component of lead-cooled fast reactors, wire-wrap spacers have the following four functions: (1) determining the spacing between neighboring fuel rods, (2) reducing the vibration of fuel rod bundles, (3) enhancing the transverse mixing of coolant and evening out the temperature gradient, (4) making the reactor core more compact and reducing the construction cost of reactor systems. Lead or lead-bismuth eutectic (LBE) operates at high temperatures and is opaque. This makes it challenging to carry out hydraulic experiments with LBE. However, model test results can be extrapolated to prototype phenomenon using similarity principle and dimensional analysis, provided that the test section is properly designed and an appropriate working fluid is selected [4]. Optical velocimetry methods, for example, particle image velocimetry (PIV) [5–7] were commonly employed in model tests to study flow characteristics in fuel bundle channels. Research into the flow characteristics within wire-wrapped fuel bundle channels is a very challenging topic, and the difficulties are [8]: (1) precision machining of visualization fuel assembly models; (2) imaging within narrow flow channels; (3) capturing rotational motion; (4) managing laser stray light interference; (5) limited lifespan of visualization fuel assembly model; (6) ensuring material compatibility; (7) maintaining material stability; (8) demanding high equipment performance standards; (9) addressing multidisciplinary issues; (10) generating grid structures for the contact line region between wire-wrap spacers and fuel rods.

Computational fluid dynamics (CFD) is a common tool to study the flow velocity distribution due to its low cost and high accuracy. However, these CFD simulation results still require validation through experimental data. Over the past few decades, many studies have been conducted to explore the flow behavior within wire-wrapped fuel bundle channels, employing both numerical simulations and experimental approaches.

(1) Numerical research: Gajapathy et al. [9] simulated the flow characteristics in 7, 19, and 37-pin wire-wrapped fuel assemblies of the Indian prototype fast breeder reactor by CFD method using the standard k-ε model. The simulation findings were benchmarked against those of 91-pin experiments

* Supported by the Large Research Infrastructures China initiative Accelerator Driven System (No. 2017-000052-75-01-000590), and Study on the Transverse Mixing Model of Subchannel in Wire-wrapped Fuel Bundles based on CFD and PIV (No. 2023A1515110809).
† Corresponding author1, Sicheng Wang, wangsicheng@impcas.ac.cn
‡ Corresponding author2, Han Wang, wanghan@ncepu.edu.cn

and agreed well. Flow velocity results of the 19 and 37-pin models differed little. The authors expected the distribution of velocity and temperature could be applied to 217-pin bundle fuel assembly. Rolfo et al. [10] studied 7, 19, 61, and 217-pin fuel assemblies with spiral wire-wrap spacers using the standard k-ε model and second-moment closure turbulent model in 2012. They found that the main flow structure in four fuel assemblies was almost the same. The number of rods had little influence on the CFD results. The results of the two turbulent models agreed well with each other and the experiment correlations, especially that of Cheng and Todreas [11]. Brockmeyer et al. [12] used the Shear Stress Transport (SST) k-ω model and elliptic blending k-ε turbulent models to study flow characteristics in 19, 37, 61, and 91-pin wire-wrapped bundles in 2017. The CFD results were validated by those of Large Eddy Simulation (LES). Their study indicated that the main flow velocity in central subchannels changed with the number of rods. However, some flow characteristics such as vortices and transverse velocities were independent of the increase of the number of rods. Zhao et al. [13] performed CFD of a 7-pin wire-wrapped fuel assembly with different shapes of duct walls using the SST model which can switch to the k-ε model. The results were compared with those of LES of Argon National Laboratory and experiments and matched well. Also, they found that the duct wall shape can affect the flow characteristic in the subchannels. Overall, CFD numerical simulations have validated the coherence and similarity of flow characteristics in 7, 19, 37,61, and even 217-pin wire-wrapped fuel assemblies. This can help in the simplification of experiment studies. Many existing CFD studies [12–16] suggested the use of SST k-ω model for simulating fuel assemblies with spiral wires.

(2) Experimental research: Polymethyl methacrylate (PMMA) and sodium iodide solution, fluorinated ethylene propylene (FEP) and deionized water, are commonly used as model material and refractive index matching (RIM) fluid combination, in PIV experiment, more RIM schemes can be found in this research [17]. Nguyen et al. [18] performed PIV experiments in a 61-pin wire-wrap bundle model using PMMA and p-cymene in 2017. They measured the flow velocity near rods and wire-wrap spacers under a Reynolds number of 19000 and observed that the large-scale structures were oriented parallel with the mean flow direction. Goth et al.[19] performed PIV measurements on the flow field distribution of multiple interior subchannels in a 61-pin wire-wrapped fuel assembly with a Reynolds number of 19000 in 2018, these results can serve as benchmarks for CFD simulations. Wang et al.[20] executed the PIV experiment in a single rod model with spiral wires. They studied the cross flow in the cross-section and found that both the velocity magnitude in cross-sections increased gradually a rise in the Reynolds number, as indicated by the experimental results. Zhang et al. [21] conducted the PIV experiment and CFD simulation in a 7-pin wire-wrapped fuel assembly at a Reynolds number of 6500 in 2020. They captured the flow distribution in the cross-section of the test secion. Through experiments, the axial and transverse velocity distribution and RMS of the transverse velocity fluctuation. They found that the CFD simulation using the SST model could accurately predict well the flows in a 7-pin fuel assembly. Additionally, they observed that different locations and the number of wires in different subchannels influenced the turbulent characteristics. Bovati and Hassan [22] performed LES with a wall function to study the effect of local blockage accidents in a 61-pin wire-wrapped fuel assembly at a Reynolds number of 17000 in 2022. The mean velocity and RMS fluctuating velocity results were compared with existing PIV data. The LES model showed its capability to simulate the pair of counter-rotating vortices. Li et al. [23] conducted PIV and CFD studies in a 7-pin wire-wrapped fuel assembly in CiADS in 2023. The CFD results demonstrated the SST models proficiency to predict the vortex formation near wire-wrap spacers in cross-sections. Similarly, Sun et al. [24] studied the cross-flow in a 7-pin wire-wrapped fuel bundle by PIV and CFD methods, using FEP and deionized water. They found that the cross-flow has obvious periodicity, and the peak ratio of transverse velocity to axial velocity was 25%. Wang et al. [25] performed PIV measurements in a 7-pin wire-wrapped bundle with FEP and deionized water in 2023. The experiment results revealed the strong circulation flow in the outer region of the test section. The velocity of circulation flow was about 35% of the streamwise velocity. These conclusions are consistent with those reported in previous studies [8, 23].

Most of the previous studies concentrated on the general flow feature in the wire-wrapped fuel assembly and only a few researches paid attention to detailed local velocity distributions. This study aimed to further evaluate the transverse velocity in wire-wrapped fuel bundle channels and enhance the safety performance of the CiADS. This will help to deepen the research on the transverse mixing phenomenon and the mechanism of coolant under the influence of wire-wrap spacers and provide strong support for the design of lead-cooled fast reactors.

II. PIV STUDY

In this paper, PMMA was chosen as the material for the test section, and a 62.932 wt% sodium iodide-36.968 wt% deionized water-0.1 wt% sodium thiosulfate solution was prepared as the RIM fluid [17]. The velocity distribution of the fuel bundle channel was investigated by PIV. The image resolution of the CCD camera was 6600×4400 pixels, and the laser pulse energy was 200 $\mathrm{mJ/pulse}$. A synchronizer controls the CCD camera and laser, making sure they work at the same time. The laser was scattered into a light sheet by the optical lens. Tracer particles reflect this light sheet and can be captured by the CCD camera. Two consecutive frames, named frame A and frame B, were captured between certain time interval Δt. The displacements of tracer particles were determined using algorithm to obtain the velocity vectors. The velocity distribution of trace particles can represent that of the working liquid when the tracer particles' following capability is ensured.

A. Test section

Fig. 1 shows a picture of the 19-pin fuel assembly model. The bottom end plugs were made of 316L stainless steel for easy assembling, enhancing mechanical strength, and providing corrosion resistance. In this study, SP stands for the starting point of the wire-wrap spacers, while 1R represents row 1, and the abbreviation rules for other rows were similar. Wire-wrap spacers were wrapped on the fuel rods using a self-designed gear-synchronized positioning device [26, 27].

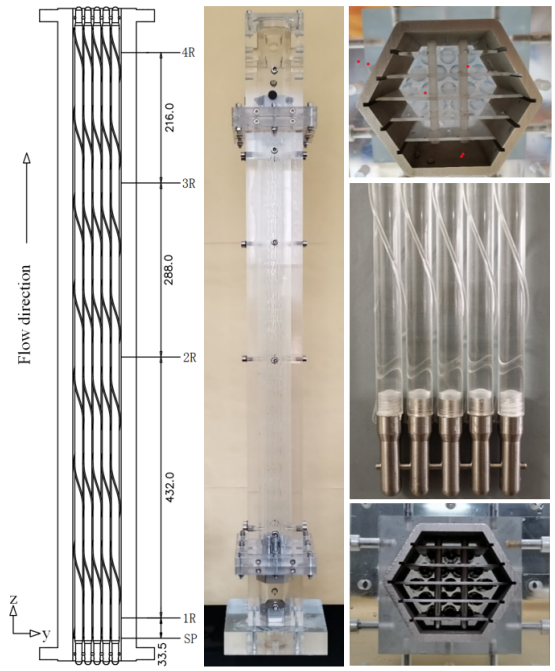

Fig. 1. Picture of the 19-pin wire-wrapped fuel assembly model.

The diameters of the fuel pins and wire-wrap spacers were designed to be the same as those in CiADS. The primary parameters of the visualized fuel assembly model are shown in Table 1.

Table 1. Primary parameters of the visualized fuel assembly.

Item	Paramter
Number of fuel rods	19
Diameter of fuel rods, mm	12.995
Length of fuel rods, mm	1089
Fuel rod arrangement	triangular
Diameter of the wire-wrap spacer, mm	2.005
Lead pitch of the wire-wrap spacer, mm	144
Number of lead pitches	7
Rotation direction of the wire-wrap spacer	clockwise
Inner side length of the duct, mm	40.373
Outer side length of the duct, mm	130
Length of the duct, mm	1540

B. Experimental Platform

As shown in Fig. 2, a Visual Hydraulic ExperimentaL Platform (VHELP) was designed and assembled [8, 28] which included a primary loop and a secondary loop. The secondary loop regulated the temperature of working liquid inside the primary loop. Tank 3 was the highest point of the platform, which was used for adding tracer particles, draining bubbles, reducing pressure fluctuations, and monitoring the liquid level. To reduce the refractive index differences between the fuel bundle model and the working liquid, a sodium iodide solution was formulated with a concentration of 62.932%. This solution exhibited a refractive index of 1.491 at 25°C (same as that of the PMMA). The RIM fluid traversed the test section in an upward direction, originated from the bottom, and worked at the range of 25 ± 1.0°C, under atmospheric pressure. To accommodate different experimental conditions and enhance measurement precision, two turbine flowmeters were installed in parallel in the primary loop. These flowmeters have measuring ranges of 1.5-15 $\mathrm{m^3/h}$ and 4.0-40 $\mathrm{m^3/h}$, respectively. At the same time, a vortex flowmeter covering a range of 5.0-50 $\mathrm{m^3/h}$ was also employed. Thermocouples and gauge pressure sensors were strategically installed to facilitate continuous monitoring and ensure the working liquid's physical properties.

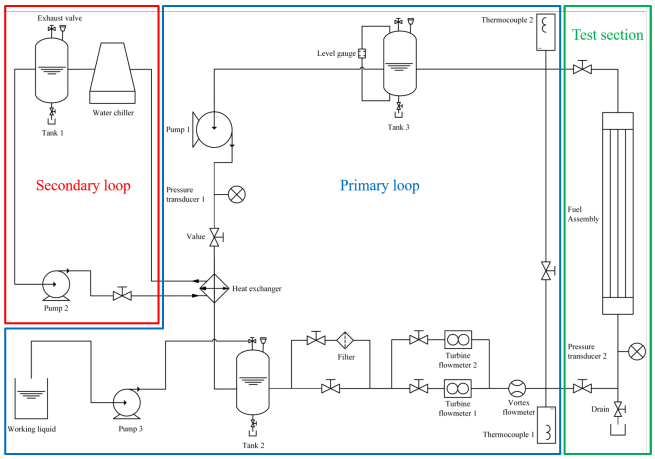

Fig. 2. Diagram of the Visual Hydraulic ExperimentaL Platform (VHELP).

The variations in refractive index, density, and dynamic viscosity of the 62.932% sodium iodide solution at a temperature at 25°C were meticulously measured. The variation relations are presented in equations (1), (2), and (3).

$$n_T = -1.31130 \times 10^{-4} T + 1.49530, \mathrm{R}^2 = 0.9833 \quad (1)$$

where n_T is the refractive index, T is the temperature, °C.

$$\rho_T = -7.02779 \times 10^{-4} T + 1.88532, \mathrm{R}^2 = 0.9937 \quad (2)$$

where ρ_T is the density, $\mathrm{g/cm^3}$, T is the temperature, °C.

$$\mu_T = -1.03047 \times 10^{-12} T^6 + 3.34261 \times 10^{-9} T^4 - 4.29940 \times 10^{-6} T^2 + 0.00423, \mathrm{R}^2 = 0.9993 \quad (3)$$

where μ_T is the dynamic viscosity, $\mathrm{Pa \cdot s}$, T is the temperature, $^\circ\mathrm{C}$.

The density of the 62.932% sodium iodide solution at 25 $^\circ\mathrm{C}$ was 1.868 $\mathrm{g/cm^3}$. This value was similar to that of the tracer particle, which has a density of 1.7 $\mathrm{g/cm^3}$ and an average diameter of 7 $\mu\mathrm{m}$. This similarity ensured the desired following behaviors of the tracer particle.

Fig. 3 shows the layout of the PIV system. The laser transmitter and CCD camera were arranged in two perpendicular directions of the test section. The aluminum alloy support was covered with light-absorbing cloth, and the rest zone was coated with matte paint, to reduce the stray light interference. Adjust the level and verticality of the electric lifting platform, and pay attention to the parallel relationship between the electric lifting platform and the fuel assembly. Fig. 4 shows a top view of the channels in the xz plane. According to the position of the laser sheet along the y-axis of the fuel assembly model, the photographing flow channels were designated as gaps 1 through 5, respectively. Each gap was parallel to the xz plane and crossed the diameter of rods and the wire-wrap spacers.

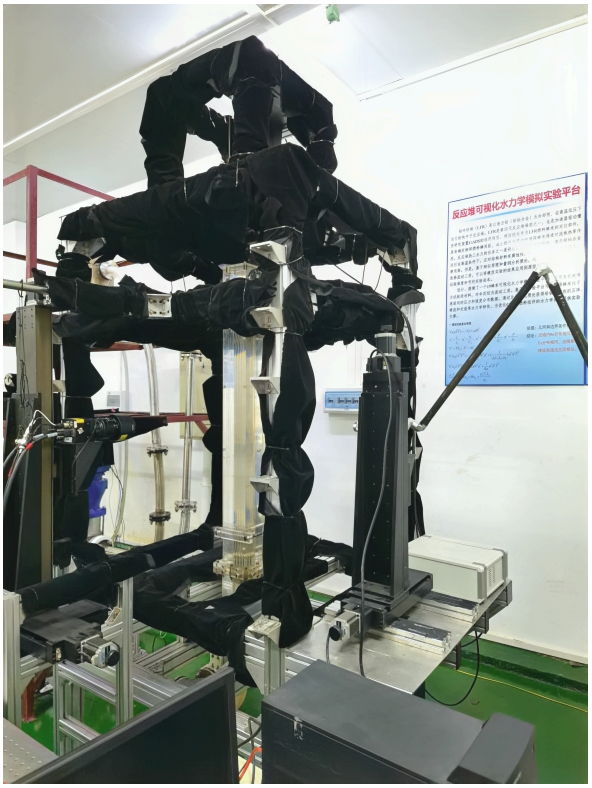

Fig. 3. Physical Picture of the PIV layout

The velocity distributions in the xz plane at 2.25-3.25 pitches (H) and 3.75-4.75 H were measured by PIV, respectively. A set of motion controller was used to adjust the light sheet and CCD camera with the height range of fuel assembly, spanning from 2.25 to 3.25 H. Subsequently, the velocity distributions in each channel were captured under four working conditions with Reynolds numbers of 2500, 3750, 5000 and 6250. After that, the CCD camera and the laser light were lifted synchronously by 216 mm (1.5 H), and the velocity distributions at the 3.75-4.75 H channel were measured.

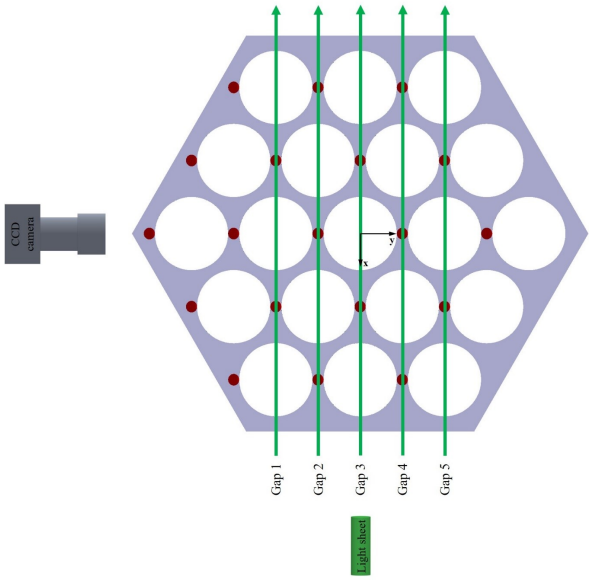

Fig. 4. Top view of channels in the xz plane

III. CFD STUDY

Normally, experimental measurements can only provide restricted and macroscopic data, whereas numerical simulations can provide quite a lot of microscopic flow characteristics, to further validate the applicability of CFD computational models and improve the credibility of experimental data. This research utilized FLUENT for simulating flow characteristics. FLUENT has strong grid adaptability, containing a large number of solving algorithms and rich turbulence models. It is one of the most widely applicable commercial software currently available.

CATIA P3 V5-6R software, developed by the Dassault System, was utilized to generate the 3D model of the flow channel, as shown in Fig.5. The presence of line contact and sharp edges poses significant challenges in grid generation. To mitigate these difficulties, a wire-wrap spacer was indented by 0.1 mm towards its fuel rod, and a fillet radius of 0.25 mm was incorporated to simplify the grid generation process. Previous studies have shown that this geometric simplification has a negligible effect on the flow characteristics in a wire-wrapped fuel bundle channel [29–32]. STAR-CCM+ software, developed by CD-adapco, featuring powerful mesh generation tools and its greatest advantage lies in its ability to produce high-quality polyhedral meshes. STAR-CCM+ 19.0 was utilized to create a polyhedral mesh, which, in contrast

to a tetrahedral mesh, offers advantages such as reduced cells and a accelerated convergence rates. Fig. 6 illustrates the grid distribution at the entrance of fuel rod bundle. There were four boundary layers in the mesh, each with a height of 0.025 mm. FLUENT has strong grid adaptability, contains a large number of solving algorithms and rich turbulence models, and is one of the most widely applicable commercial software currently available. FLUENT 19.2 was used to carry out numerical simulation of the fuel bundle channels, and the parameter settings were: a basic grid of 1.5 mm, four boundary layers were divided on the fuel rod and wire-wrap spacer surface, the velocity inlet and pressure outlet boundary conditions, and SST k-ω turbulence model and SIMPLE algorithm were selected [33–35], and the turbulence intensity was set as 5%.

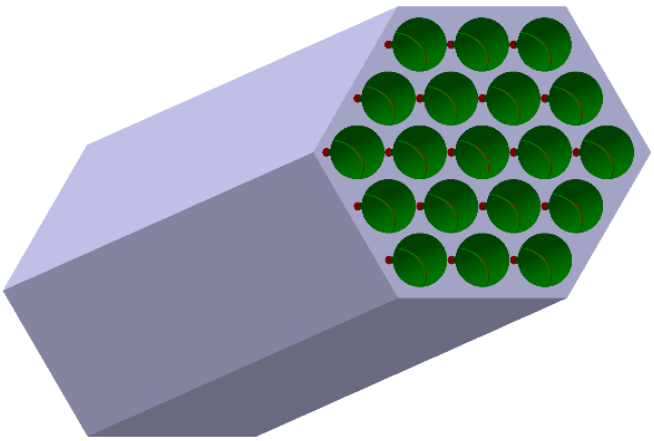

Fig. 5. Three-dimensional model of the flow channel

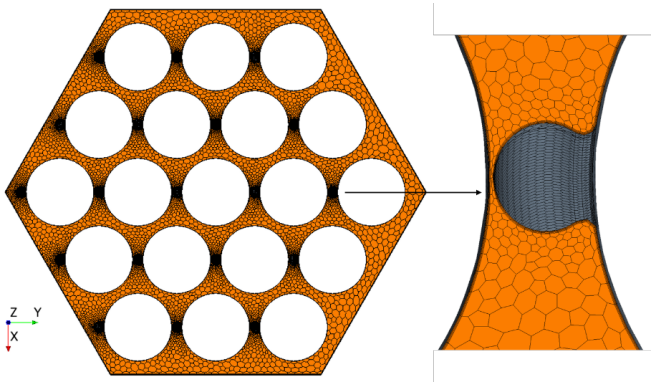

Fig. 6. Topview of the grid distribution

Fig. 7 shows the contour image of velocity distribution along the flow direction from 3.0 H to 3.0 and 5/6 H at an interval of 1/6 H when the Reynolds number was 5000. It can be seen that for every 1/6 H increase in the axial height, the contour image of velocity distribution rotates clockwise by 60°, and the value remained consistent, indicating that the transverse periodicity of the velocity distribution is one H. Fig. 8 shows the result of mesh sensitivity analysis and different meshes are consistent with each other. Finally, the mesh of 1.5mm was chosen for a balance between accuracy and computational cost.

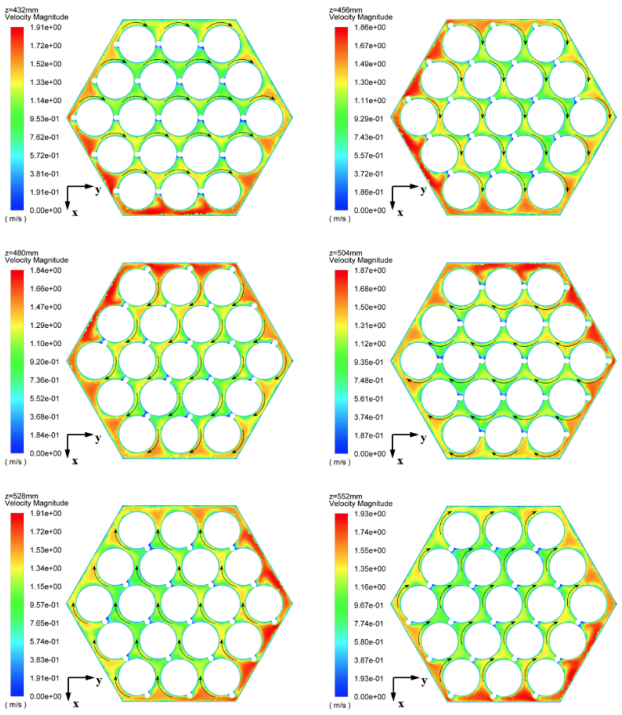

Fig. 7. Contour images of the velocity distribution on the cross-sections from 3H to $3\frac{5}{6}$H at intervals of $\frac{1}{6}$H

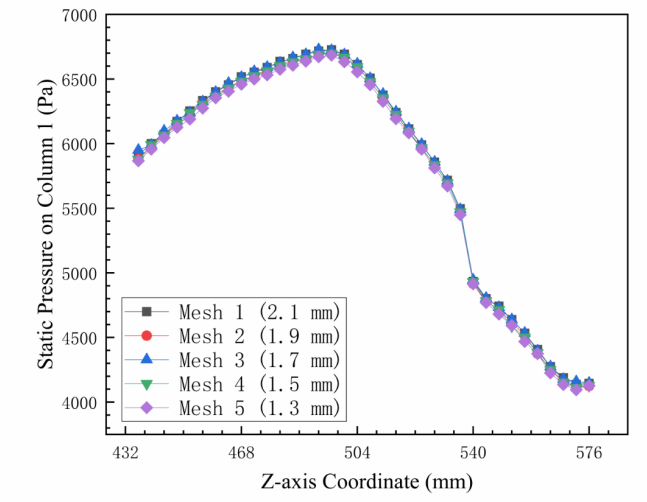

Fig. 8. Mesh sensitivity study

IV. RESULTS AND DISCUSSION

The RMS transverse velocity can be used to assesses the effective value of the transverse velocity, with its expression given as:

$$U_{\mathrm{RMS}} = \sqrt{\frac{1}{n}\sum_{i=1}^{n} U_i^2} \tag{4}$$

where U_{RMS} is the RMS transverse velocity in the xz plane, $\mathrm{m/s}$, and U is the transverse velocity in the xz plane, $\mathrm{m/s}$.

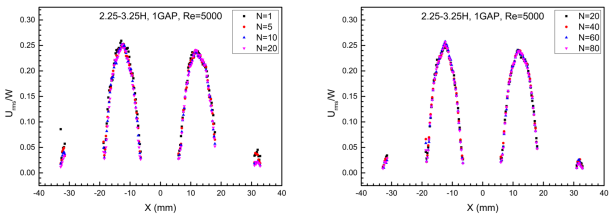

Fig. 9. The relationship between the ratio of RMS transverse velocity to the axial velocity of the fuel bundle on gap 1 and number of captures

The impact of the number of two frames (frames A and B) on the velocity vector during each capture was studied. Fig. 9 compares the relationship between the ratio of RMS transverse velocity to axial velocity of fuel bundle on gap 1 and the number of captures when the Reynolds number was 5000. The number of two frames was 1, 5, 10, 20, 40, 60 and 80 pairs, respectively. It was evident that when the number of captures at a time exceeded 40, the ratio changed little, thus 40 pairs of image frames were captured and post-processed each time to compute the average value, which helps reduce experimental errors.

A. Velocity contour images

Fig.10 shows the comparison of experimental and simulation results of transverse velocity contour images on gap 1 at 2.25-3.25H (SP was the zero point of the z-axis) in the xz plane at different Reynolds numbers. The x-axis velocity was represented by U, and the z-axis velocity was represented by W. Positive values represent flow along the positive half-axis, while negative values represent flow along the negative half-axis. It was evident that the transverse flow velocity on gap 1 increases in proportion to Reynolds numbers, and the flow contour images were similar at four conditions. The flow downstream of the wire-wrap spacers changes dramatically with micro transverse flows observed in close proximity to the wire-wrap spacers. Simultaneously, it was found that the trend of simulation results aligned closely with that of experimental data, and the values were generally equal, indicating that the SST k-ω model accurately simulate the velocity distribution within the wire-wrapped fuel bundle channels.

Fig.11 shows the comparison of PIV results of transverse velocity contour images on five gaps at 2.25-3.25 H and 3.75-4.75 H at the Reynolds number of 5000, respectively. It was evident that the transverse velocity contour images of the top-half pitch and the bottom-half pitch on gap 1 within 2.25-3.25 H were similar to that of the bottom-half pitch and top-half

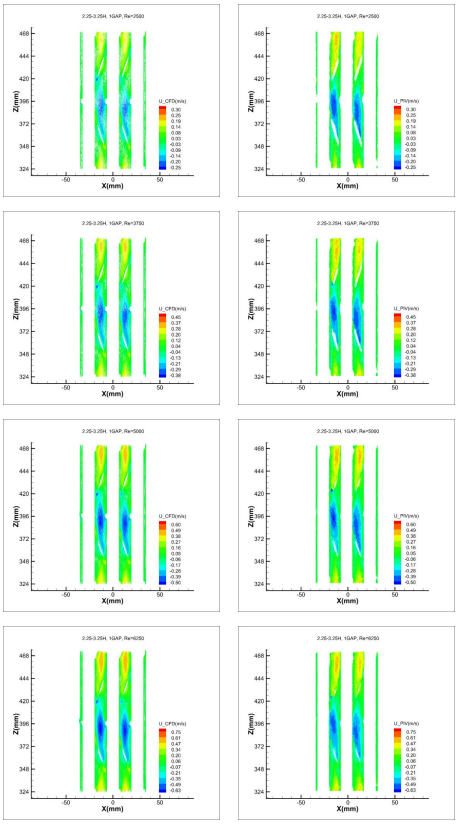

Fig. 10. Experimental and simulation results of transverse velocity contour images on gap 1 in the xz plane at 2.25-3.25 H at different Reynolds numbers

pitch on gap 1 at 3.75-4.75 H, respectively, so were those on other four gaps. At the same time, the pattern of transverse velocity contour images on gap 1, gap 2, gap 3, gap 4, and gap 5 at 2.25-3.25 H were symmetrical to that at 3.75-4.75 H on gap 5, gap 4, gap 3, gap 2, and gap 1, respectively, with opposite values, that is, the maximum and minimum values at the same position were exchanged. This was because gap 1 at 2.25-3.25 H and the gap 5 at 3.75-4.75 H were symmetrical at about the y=0 plane, and the axial difference was half a pitch. Furthermore, it was found that the transverse velocity contour images in the middle two channels on gap 1, gap 3, and gap 5 were similar, with drastic changes along the flow direction; and the transverse velocity contour images in the leftmost and rightmost channels were similar, with little variation along the direction of flow. The transverse velocity contour images in the leftmost and rightmost channels on gap 2 and gap 4 were similar, and the magnitude and changes of those in the left, middle, and right channels were quite close.

Fig.12 shows the comparison of PIV results of axial velocity contour images on five gaps at 2.25-3.25 H and 3.75-4.75 H at the Reynolds number of 5000, respectively. It can be seen that the axial velocity contour images of the top-half

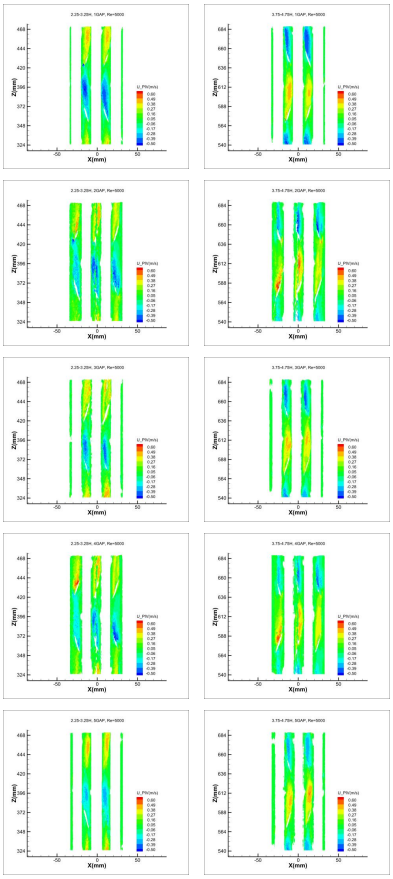

Fig. 11. Comparison of the PIV results of transverse velocity contour images on the five gaps in the xz plane at 2.25-3.25 H and 3.75-4.75 H when Reynolds number was 5000

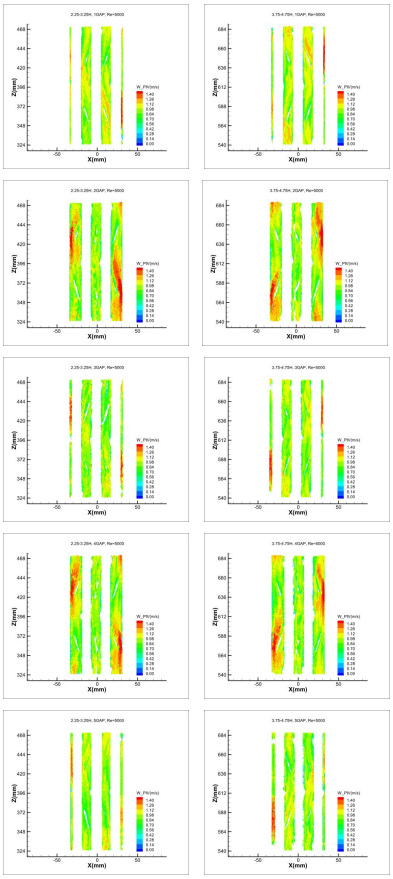

Fig. 12. Comparison of the PIV results of the axial velocity contour images on the five gaps in the xz plane at 2.25-3.25 H and 3.75-4.75 H when Reynolds number was 5000

pitch and the bottom-half pitch on gap 1 within 2.25-3.25 H were similar to that of the bottom-half pitch and top-half pitch on gap 1 at 3.75-4.75 H, respectively, and the trends on other four gaps were similar, indicating that the axial periodicity of velocity distribution was one pitch. Meanwhile, the pattern of axial velocity contour images on gap 1, gap 2, gap 3, gap 4, and gap 5 at 2.25-3.25 H were symmetrical to that at 3.75-4.75 H on gap 5, gap 4, gap 3, gap 2, and gap 1, respectively, and the values were essentially equal. This was because gap 1 at 2.25-3.25 H and the gap 5 at 3.75-4.75 H were symmetrical at about the y=0 plane, and the axial difference was half a pitch. At the same time, it was found that the axial velocity contour images in the middle two channels on gap 1, gap 3, and gap 5 were similar, with drastic changes along the flow direction; and the axial velocity contour images in the leftmost and rightmost channels alternated in magnitude. The axial velocity contour image changes in the leftmost and rightmost channels on gap 2 and gap 4 were more drastic than those in the middle channel. This disturbance in the flow was attributable to the presence of the hexagonal duct, with a notably pronounced effect noted in the vicinity of wire-wrap spacers.

Combining with Fig.11 and Fig.12, it can be seen that the period of axial velocity distribution and transverse velocity distribution is one pitch.

B. RMS transverse velocity distributions

This part analyzes the distribution of RMS transverse velocity with Reynolds number, for a quantitative analysis of the cross-flow characteristics. Fig.13 shows the variation of RMS transverse velocity with x-axis coordinates at different Reynolds numbers. It can be seen that the RMS transverse velocity increases in proportion to the rise in Reynolds numbers, and the PIV results were consistent with the CFD data.

Fig.14 illustrates the RMS transverse velocities on different gaps within 2.25-3.25 H and 3.75-4.75 H at the Reynolds number of 5000, respectively. It can be observed that on gap 1, gap 3, and gap 5 were approximately, so were those on gap 2 and gap 4, which is consistent with the findings in Fig.11. Simultaneously, it was discovered that the transverse flow in the middle two channels on gap 1, gap 3, and gap 5 was greater, while that in the leftmost and rightmost channels was

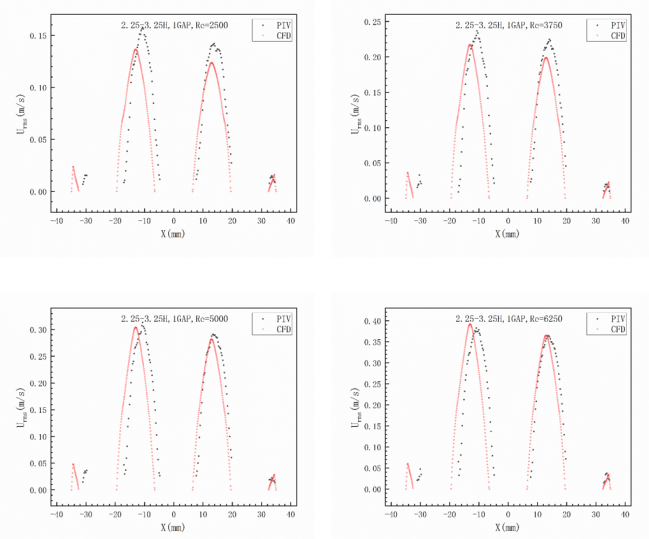

Fig. 13. Comparison of RMS transverse velocity distribution on gap 1 in the xz plane within 2.25-3.25 H at various Reynolds numbers

smaller. The magnitude of transverse flow in the left, middle, and right channels on gap 2 and gap 4 were comparable. In addition, the scatters at 2.25-3.25 H and 3.75-4.75 H on these five gaps almost overlap, this was because the transverse velocity distribution in the top and bottom half pitches at 2.25-3.25 H was similar to that of the bottom and top half pitches at 3.75-4.75 H, respectively. The results obtained from CFD were in good agreement with the PIV data, and the position of vectors with high transverse velocity on the x-axis was basically the same. The two-peak velocity distributions observed on gap 2 and gap 4 were due to the narrow gap between the two symmetric and separate parts of hexagonal ducts. The ducts were connected by a very thin layer of glue, which was a necessary processing step. This processing method has a minor effect on the PIV images.

C. Normalized transverse velocity distributions

This section analyzes the distribution of normalized transverse velocity with Reynolds number and gap position, respectively. Fig.15 shows the numbering of fuel rod and subchannel in a 19-pin wire-wrapped fuel bundle channel, comprising inner subchannels, edge subchannels, and corner subchannels.

The normalized transverse velocity at the centerline of two subchannels interface can be used to characterize the transverse mixing intensity between adjacent subchannels, and its expression is:

$$U_t = \frac{U}{W_{bulk}} \tag{5}$$

where U_t represents the normalized transverse velocity, U is the transverse velocity at the centerline of subchannel interface, $\mathrm{m/s}$, and W_{bulk} represents the axial bulk velocity of the fuel bundle, $\mathrm{m/s}$.

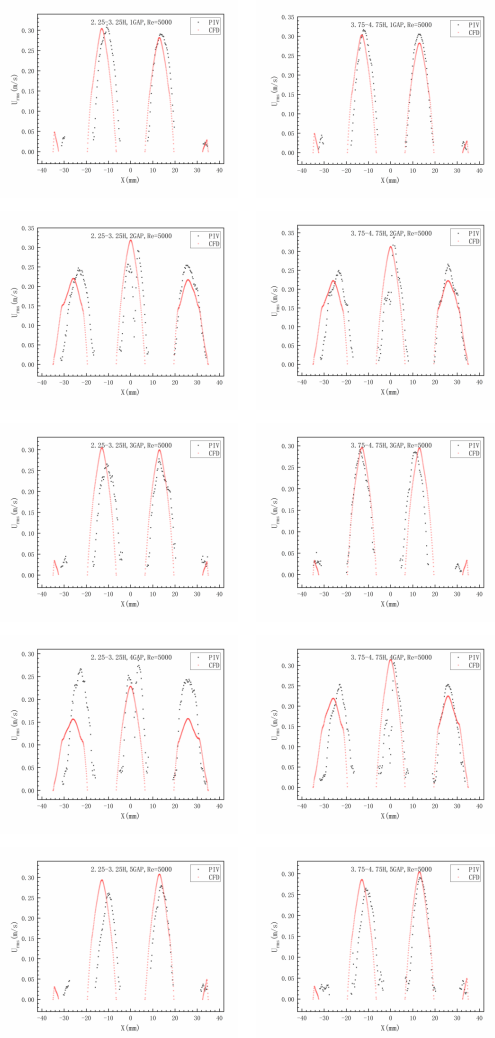

Fig. 14. Comparison of RMS transverse velocity distributions on different gaps in the xz plane at 2.25-3.25H and 3.75-4.75H at the Reynolds number of 5000

Fig.16 shows the comparison of normalized transverse velocity distribution on the interface of subchannels 19 # to 18 # at 2.25-3.25 H at different Reynolds numbers. It was evident that the value of U_t was independent of Reynolds numbers, indicating that U increases proportionally with Reynolds numbers. As the z-axis coordinate increases, U_t changes in a cosine function, with a maximum value of about 40% and a peak occurring at a position slightly behind 3/4 H. The cross-flow around the wire-wrap spacers was enhanced, and there was a deviation in the direction of velocity. Concurrently, the CFD results aligned well with the PIV data.

Fig.17 shows the normalized transverse velocity distribution on the interfaces of different subchannels in the xz plane at 2.25-3.25 H and 3.75-4.75H when the Reynolds number was 5000. It can be seen that the values of U_t at the interface of two subchannels 19# -18# and 23# -22# were equal

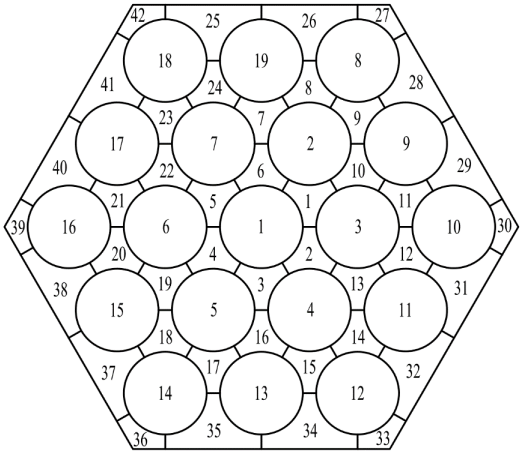

Fig. 15. Three types of subchannels and their numbers

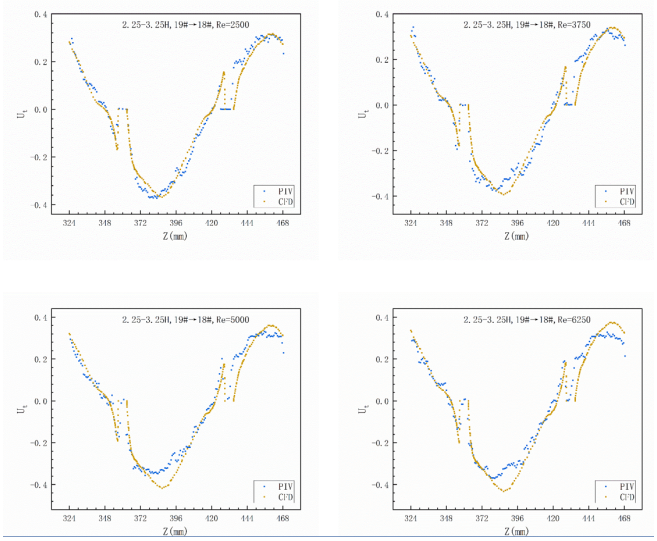

Fig. 16. Comparison of normalized transverse velocity distributions on the interfaces of subchannels 19 # to 18 # in the xz plane at 2.25-3.25H at different Reynolds numbers

at 2.25-3.25 H and 3.75-4.75 H, with opposite trends. At the same time, it was found that the transverse velocity distribution of 19# -18# and 23# -22# at a same height was basically consistent, consistent with the conclusion of the transverse velocity contour images in Fig.11 .

V. CONCLUSION

In this study, PIV and FLUENT were utilized to study the flow velocity distribution on different gaps in the xz plane at 2.25-3.25 H and 3.75-4.75 H in a 19-pin wire-wrapped fuel assembly. The axial and transverse velocity contour images of different fuel bundle gaps at various Reynolds numbers were presented. Meanwhile, RMS transverse velocity distribution and normalized transverse velocity distribution were analyzed to quantify the transverse flow characteris-

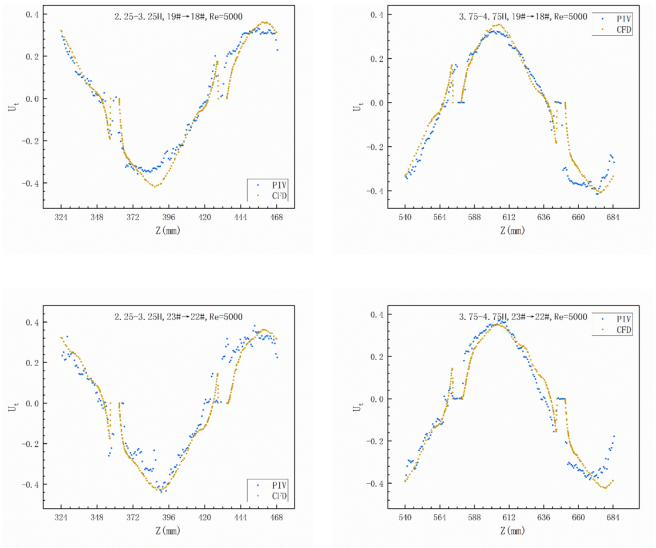

Fig. 17. Comparison of normalized transverse velocity distributions on the interfaces of different subchannels in the xz plane at 2.25-3.25 H and 3.75-4.75 H when Reynolds number was 5000

tics and validate CFD results, the following conclusions were reached:

(1) The SST k-ω model can precisely describe the velocity distribution in a wire-wrapped fuel assembly. For every 1/6 H increase in axial height, ranging from 3.0 to 4.0 H, the direction of velocity image contour rotated clockwise by 60 degrees, maintaining its magnitude unchanged. This behavior demonstrated both the transverse and axial periodicity of velocity distribution was one pitch.

(2) The flow velocity distribution patterns remained consistent as Reynolds numbers rose. However, the magnitude of these velocities increased in direct proportion to the rise in Reynolds number. The flow downstream of wire-wrap spacers underwent significant changes, accompanied by the emergence of micro transverse flows in their vicinity.

(3) The RMS transverse velocity increased proportionally with Reynolds numbers. The values of U_{RMS} on gap 1, gap 3, and gap 5 was essentially equal, so were those on gap 2 and gap 4. The cross-flow in the middle two channels on gap 1, gap 3, and gap 5 were greater whereas that in the leftmost and rightmost channels were smaller. The magnitude of cross-flow in the left, middle, and right channels on gap 2 and gap 4 were comparable. In addition, the curves on these five gaps at 2.25-3.25 H and 3.75-4.75 H almost overlapped.

(4) The value of U_t remained constant regardless of Reynolds number, signifying that U increases proportionally with Reynolds number. As the z-axis coordinate increased, U_t changed in a cosine function, with maximum amplitude of approximately 40% and a peak occurring at a position slightly behind 3/4 H. The cross-flow around wire-wrap spacers was enhanced, and there was a deviation in the direction of velocity.

The findings and conclusions in this study can help deepen the research on the transverse mixing phenomena and its un-

derlying mechanisms of coolant in the presence of wire-wrap spacers and provide strong support for the safety assessments of lead-cooled fast reactors.

[1] W.L. Zhan, H.S. Xu, Advanced Fission Energy Program - ADS Transmutation System. Bull. Chin. Acad. Sci.,**27**, 375-381 (2012). (in Chinese).

[2] L. Gu, X.K. Su, Latest research progress for LBE coolant reactor of China initiative accelerator driven system project. Front. Energy 15, 22 (2021). doi.org/10.1002/er.6569

[3] R. Yu, L. Gu, X. Sheng et al., Review of fuel assembly design in lead-based fast reactors and research progress in fuel assembly of China initiative accelerator driven system. Int. J. Energy Res. 45, 11552-11563 (2021). doi.org/10.1002/er.6569

[4] L.I. Sedov, Similarity and Dimensional Methods in Mechanics. 10th edn, (CRC Press,1993). https://www.researchgate.net/publication/268530405 Similarity and dimensional methods in mechanics Transl from the Russian by V I Kisin

[5] R.D. Keane, R.J. Adrian, Optimization of particle image velocimeters. I. Double pulsed systems. Meas. Sci. Technol. 1, 1202-1215, (1990). doi.org/10.1088/0957-0233/1/11/013

[6] R.D. Keane, R.J. Adrian, Optimization of particle image velocimeters: II. Multiple pulsed systems.Meas. Sci. Technol. 2, 963-974, (1991). doi.org/10.1088/0957-0233/2/10/013

[7] J. Westerweel, G.E. Elsinga, R.J. Adrian, Particle Image Velocimetry for Complex and Turbulent Flows. Annu. Rev. Fluid Mech. 45 (2013): 409-436. doi.org/10.1146/annurev-fluid-120710-101204

[8] D.J. Fan, Study on the Flow Characteristics of Wire-wrapped Fuel Bundle Channel in a Lead-cooled Fast Reactor, University of Chinese Academy of Sciences, (2021). (in Chinese). doi.org/10.27560/d.cnki.gkjwc.2021.000054

[9] R. Gajapathy, K. Velusamy, P. Selvaraj et al., A comparative CFD investigation of helical wire-wrapped 7, 19 and 37 fuel pin bundles and its extendibility to 217 pin bundle. Nucl. Eng. Des. 239, 2279-2292, (2009). doi.org/10.1016/j.nucengdes.2009.06.014

[10] S. Rolfo, C. Péniguel, M. Guillaud et al., Thermal-hydraulic study of a wire spacer fuel assembly. Nucl. Eng. Des. 243, 251-262, (2012). doi.org/10.1016/j.nucengdes.2011.11.021

[11] S.K. Cheng, N.E. Todreas, Hydrodynamic models and correlations for bare and wire-wrapped hexagonal rod bundles Bundle friction factors, subchannel friction factors and mixing parameters. Nucl. Eng. Des. 92, 227-251, (1986). doi.org/10.1016/0029-5493(86)90249-9

[12] L. Brockmeyer, L.B. Carasik, E. Merzari et al., Numerical simulations for determination of minimum representative bundle size in wire wrapped tube bundles. Nucl. Eng. Des. 322, 577-590, (2017). doi.org/10.1016/j.nucengdes.2017.06.038

[13] Y.Y. Zhao, M. Huang, J.Y. Huang et al., CFD investigation for a 7-pin wire-wrapped fuel assembly with different shapes of fuel duct wall. Ann. Nucl. Energy, 2020. doi.org/10.1016/j.anucene.2019.107272

[14] X. Chai, X.J. Liu, J.B. Xiong et al., Numerical investigation of thermal-hydraulic behaviors in a LBE-cooled 19-pin wire-wrapped rod bundle. Prog. Nucl. Energy, 2020. 119: p. 103044. doi.org/10.1016/j.pnucene.2019.103044

[15] J.J. Lin, M. Huang, S.C. Zhang et al., CFD investigation for a 7-pin wrapped-wire fuel assembly with different wires. Ann. Nucl. Energy, 2021. 164: p. 15. doi.org/10.1016/j.anucene.2021.108626

[16] J.L. Li, Y. Xiao, G.Q. Ding et al., Numerical analysis of the three-dimensional flow phenomena in a 19-pin wire-wrapped tight lattice bundle. Int. J. Heat Mass Transfer, 2022. 196: p. 14. doi.org/10.1016/j.ijheatmasstransfer.2022.123319

[17] D.J. Fan, R.J. Li, M.H. He et al., Review of refractive index-matching techniques of polymethyl methacrylate in flow field visualization experiments. Int. J. Energy Res. 2023 (2023). doi.org/10.1155/2023/3413380

[18] T. Nguyen, N. Goth, P. Jones et al., PIV measurements of turbulent flows in a 61-pin wire-wrapped hexagonal fuel bundle. Int. J. Heat Fluid Flow 65, 47-59, (2017). doi.org/10.1016/j.ijheatfluidflow.2017.03.007

[19] N. Goth, P. Jones, T.D. Nguyen et al., PTV/PIV measurements of turbulent flows in interior subchannels of a 61-pin wire-wrapped hexagonal fuel bundle. Int. J. Heat Fluid Flow 71, 295-304, (2018). doi.org/10.1016/j.ijheatfluidflow.2018.03.021

[20] H. Wang, S.Q. Wang, D.G. Lu, PIV measurements of the cross flow induced by a wrapped wire spacer. Ann. Nucl. Energy, 2020. 146: p. 107634. doi.org/10.1016/j.anucene.2020.107634

[21] C. Zhang, H.R. Ju, D.L. Zhang et al., PIV measurement and numerical investigation on flow characteristics of simulated fast reactor fuel subassembly. Nucl. Eng. Technol, 2020. 52(5): p. 897-907. doi.org/10.1016/j.net.2019.10.013

[22] O. Bovati, Y. Hassan, Analysis of the turbulent flow in a partially blocked wire-wrapped rod bundle using LES with wall functions. Int. J. Heat Fluid Flow 97, (2022).doi.org/10.1016/j.ijheatfluidflow.2022.109041

[23] R.J. Li, D.J. Fan, M.H. He et al., PIV and CFD Study on Crossflow Characteristics in a 7-Pin Wire-Wrapped Bundle Channel. Int. J. Energy Res. 2023, (2023). doi.org/10.1155/2023/5542001

[24] M.C. Sun, H. Wang, D.G. Lu, Flow-visualization Experiment and Numerical Investigation of Cross Flow in Wire-wrapped Rod Bundle. At. Energy Sci. Technol 57, 968-977 (2023). (in Chinese). doi: 10.7538/yzk.2022.youxian.0493

[25] H. Wang, M.C. Sun, D.J. Fan et al., Experimental investigation of the crossflow of water in a 7-pin wire-wrapped rod bundle. Exp. Therm. Fluid Sci. 149, 111010 (2023). doi.org/10.1016/j.expthermflusci.2023.111010

[26] D.J. Fan, L. Gu, T.J. Peng et al., Method for processing visual fuel rod of lead-cooled fast reactor. CN113643836A. 2023.08.01.

[27] D.J. Fan, L. Gu, T.J. Peng et al., Positioning device for gear synchronization and using method thereof[P]. CN113571210B. 2023.08.22.

[28] D.J. Fan, T.J. Peng, Y.Z. Tang et al., Periodicity and transversal pressure distribution in a Wirewrapped 19Pin fuel assembly. Int. J. Energy Res. 45, 11837-11850 (2020). doi.org/10.1002/er.5809

[29] W.D. Pointer, J. Thomas, T. Fanning et al., RANS-based CFD simulations of sodium fast reactor wire-wrapped pin bundles. In American Nuclear Society - International Conference on Mathematics, Computational Methods and Reactor Physics 2009, Vol. 4, pp. 22122224. https://www.mendeley.com/catalogue/dac959e6-8b9b-33fb-

9b41-c328de4ad037/
[30] E. Merzari, W.D. Pointer, J.G. Smith et al., Numerical simulation of the flow in wire-wrapped pin bundles: Effect of pin-wire contact modeling. Nucl. Eng. Des. 253, 374-386, (2012). doi.org/10.1016/j. nucengdes.2011.09.030
[31] E. Merzari, P. Fischer, H. Yuan et al., Benchmark exercise for fluid flow simulations in a liquid metal fast reactor fuel assembly. Nucl. Eng. Des. 298, 218-228 (2016).doi.org/10.1016/j.nucengdes.2015.11.002
[32] A. Ahmad, K.Y. Kim, Three-dimensional analysis of flow and heat transfer in a wire-wrapped fuel assembly. Proceedings of International Congress on Advances in Nuclear Power Plants, Vol. 5. Seoul, South Korea: ICAPP, 2005.
[33] D.J. Fan, R.J. Li, R.X. Qiu et al., Applicability of RANS models and pressure drop in edge subchannels for 19-pin wire-wrapped fuel bundle channel in CiADS. Heliyon, e16203, (2023). .
[34] T. Sreenivasulu, B. Prasad, Flow and heat transfer characteristics in a seven tube-bundle wrapped with helical wires. Int. J. Adv Technol., 350-381 (2011).
[35] L. Liu, S. Wang, B.F. Bai, Thermal-hydraulic comparisons of 19-pin rod bundles with four circular and trapezoid shaped wire wraps. Nucl. Eng. Des. 318, 213-230, (2017). doi.org/10.1016/j.nucengdes.2017.04.017